

The Peculiar Transient AT2018cow: A Possible Origin of a Type Ibn/IIn Supernova

```
Danfeng Xiang<sup>1</sup>, Xiaofeng Wang<sup>1,2,3</sup>, Weili Lin<sup>1</sup>, Jun Mo<sup>1</sup>, Han Lin<sup>1</sup>, Jamison Burke<sup>4,5</sup>, Daichi Hiramatsu<sup>4,5</sup>,
       Griffin Hosseinzadeh<sup>6</sup>, D. Andrew Howell<sup>4,5</sup>, Curtis McCully<sup>4,5</sup>, Stefan Valenti<sup>7</sup>, József Vinkó<sup>8,9,10,11</sup>, J. Craig Wheeler<sup>11</sup>, Shuhrat A. Ehgamberdiev<sup>12</sup>, Davron Mirzaqulov<sup>12</sup>, Attila Bódi<sup>8,9,13</sup>, Zsófia Bognár<sup>8,9,13</sup>,
Borbála Cseh<sup>8</sup>, Ottó Hanyecz<sup>8</sup>, Bernadett Ignácz<sup>8</sup>, Csilla Kalup<sup>8</sup>, Réka Könyves-Tóth<sup>8</sup>, Levente Kriskovics<sup>8,14</sup>, András Ordasi<sup>8</sup>,
András Pál<sup>8,14,15</sup>, Krisztián Sárneczky<sup>8</sup>, Bálint Seli<sup>8</sup>, Róbert Szakáts<sup>8</sup>, T. Arranz-Heras<sup>16,17</sup>, R. Benavides-Palencia<sup>16,18</sup>
        D. Cejudo-Martínez 16,19, P. De la Fuente-Fernández 16,20, A. Escartín-Pérez 16,21, F. García-De la Cuesta 16,22, J. L. González-Carballo 16,23, R. González-Farfán 16,24, F. Limón-Martínez 16,25, A. Mantero 16,26, R. Naves-Nogués 16,27
     M. Morales-Aimar<sup>16,28</sup>, V. R. Ruíz-Ruíz<sup>16,29,30,31</sup>, F. C. Soldán-Alfaro<sup>16,32</sup>, J. Valero-Pérez<sup>16,33</sup>, F. Violat-Bordonau<sup>16,34</sup>,
                   Tianmeng Zhang<sup>35,36</sup>, Jujia Zhang<sup>37,38,39</sup>, Xue Li<sup>1</sup>, Zhihao Chen<sup>1</sup>, Hanna Sai<sup>1</sup>, and Wenxiong Li<sup>1</sup>
                Physics Department and Tsinghua Center for Astrophysics (THCA), Tsinghua University, Beijing 100084, People's Republic of China
                                                                              wang_xf@mail.tsinghua.edu.cn
                            <sup>2</sup> Beijing Planetarium, Beijing Academy of Sciences and Technology, Beijing 100044, People's Republic of China
                                 Purple Mountain Observatory, Chinese Academy of Sciences, Nanjing 210023, People's Republic of China
                                            Las Cumbres Observatory, 6740 Cortona Drive, Suite 102, Goleta, CA 93117-5575, USA
                                             Department of Physics, University of California, Santa Barbara, CA 93106-9530, USA
                                  <sup>6</sup> Center for Astrophysics|Harvard & Smithsonian, 60 Garden Street, Cambridge, MA 02138-1516, USA
                            <sup>7</sup> Department of Physics and Astronomy, University of California, 1 Shields Avenue, Davis, CA 95616-5270, USA
                  <sup>8</sup> Konkoly Observatory, Research Centre for Astronomy and Earth Sciences, Konkoly-Thege M. út 15-17, Budapest 1121, Hungary
                                 ELTE Eötvös Loránd University, Institute of Physics, Pázmany Péter sétány 1/A, Budapest 1117, Hungary <sup>10</sup> Department of Optics & Quantum Electronics, University of Szeged, Dóm tér 9, Szeged 6720, Hungary
                                               Department of Astronomy, University of Texas at Austin, Austin, TX 78712, USA
                            Ulugh Beg Astronomical Institute, Uzbekistan Academy of Sciences, Uzbekistan, Tashkent 100052, Uzbekistan

13 CSFK Lendület Near-Field Cosmology Research Group, Hungary
                                   <sup>14</sup> Eötvös Loránd University, Institute of Physics, Pázmany Péter sétány 1/A, Budapest 1117, Hungary
                              15 Eötvös Loránd University, Department of Astronomy, Pázmany Péter sétány 1/A, Budapest 1117, Hungary
16 Observadores de Supernovas Group (ObSN), Spain
                                                            <sup>17</sup> Obs. Las Pequeras, E-40470 Navas de Oro, Segovia, Spain
                                                            18 Obs. El Gallinero, E-28192 El Berruco, Madrid, Spain
20 Obs. Llanes, E-33784 Llanes, Asturias, Spain
21 Obs. Llanes, E-3384 Llanes, Asturias, Spain
                                                                   <sup>21</sup> Obs. Belako, E-48100 Mungia, Vizcaya, Spain
                                                       <sup>22</sup> Obs. La Vara MPC J38, E-33784 Muñas de Arriba, Asturias, Spain
                                                                Obs. Cerro del Viento MPC I84, E-06010 Badajoz, Spain
                                                             <sup>24</sup> Obs. Uraniborg MPC Z55, E-41400 Écija, Sevilla, Spain
                                                        Obs. Mazariegos MPC 199, E-34170 Mazariegos, Palencia, Spain
                                                               Obs. Bernezzo MPC C77, I-12010 Bernezzo, Cuneo, Italy
                                                         <sup>27</sup> Obs. Montcabrer MPC 213, E-08348 Cabrils, Barcelona, Spain
                                                       <sup>28</sup> Obs. Sencelles MPC K14, E-07140 Sencelles, Islas Baleares, Spain
<sup>29</sup> New Mexico Skies, USA
                                                                             iTelescope Siding Spring, Australia
<sup>31</sup> AstroCamp (Nerpio), Spain
                                               <sup>32</sup> Obs. Amanecer de Arrakis MPC Z74, 41500 Alcalá de Guadaira, Sevilla, Spain
                                                            Obs. Norba Caesarina MPC Z71, E-10195 Cáceres, Spain
    35 Key Laboratory of Optical Astronomy, National Astronomical Observatories, Chinese Academy of Sciences, 10101, Beijing, People's Republic of China
                   School of Astronomy and Space Science, University of Chinese Academy of Sciences, 101408, Beijing, People's Republic of China
                                     Yunnan Observatories, Chinese Academy of Sciences, Kunming 650216, People's Republic of China
       <sup>38</sup> Key Laboratory for the Structure and Evolution of Celestial Objects, Chinese Academy of Sciences, Kunming 650216, People's Republic of China
```

Abstract

³⁹ Center for Astronomical Mega-Science, Chinese Academy of Sciences, 20A Datun Road, Chaoyang District, Beijing 100012, People's Republic of China Received 2020 November 26; revised 2021 January 19; accepted 2021 January 19; published 2021 March 24

We present our photometric and spectroscopic observations of the peculiar transient AT2018cow. The multiband photometry covers from peak to \sim 70 days, and the spectroscopy ranges from 5 to \sim 50 days. The rapid rise $(t_r \lesssim 2.9 \text{ days})$, high luminosity $(M_{V,\text{peak}} \sim -20.8 \text{ mag})$, and fast decline after peak make AT2018cow stand out from any other optical transients, whereas we find that its light curves show a high resemblance to those of Type Ibn supernovae. Moreover, the spectral energy distribution remains at a high temperature of \sim 14,000 K at t > 15 days after discovery. The spectra are featureless in the first 10 days, while some broad emission lines due to H, He, C, and O emerge later, with velocity declining from \sim 14,000 to \sim 3000 km s⁻¹ at the end of our observations. Narrow and weak He I emission lines emerge in the spectra at t > 20 days after discovery. These emission lines are reminiscent of the features seen in interacting supernovae like the Type Ibn and IIn subclasses. We fit the bolometric light curves with a model of circumstellar interaction and radioactive decay of ⁵⁶Ni and find a good fit with ejecta mass $M_{\rm ej} \sim 3.16~M_{\odot}$, circumstellar medium (CSM) mass $M_{\rm CSM} \sim 0.04~M_{\odot}$, and ejected ⁵⁶Ni mass $M_{\rm 56Ni} \sim 0.23~M_{\odot}$. The CSM shell might be formed in an eruptive mass ejection of the progenitor star. Furthermore,

the host environment of AT2018cow implies a connection of AT2018cow with massive stars. Combining observational properties and the light-curve fitting results, we conclude that AT2018cow might be a peculiar interacting supernova that originated from a massive star.

Unified Astronomy Thesaurus concepts: Supernovae (1668); Circumstellar matter (241); Massive stars (732); Binary stars (154); Magnetars (992); Time domain astronomy (2109); Optical observation (1169)

Supporting material: data behind figure, machine-readable table

1. Introduction

The studies of time-domain astronomy cover a variety of optical transients, including novae, supernovae (SNe), tidal disruption events (TDEs), kilonovae, etc. With different physical origins, these transients exhibit a huge diversity in evolutionary properties, especially optical light curves. The evolutionary timescales and luminosities of different transients are directly related to their physical origins. There is a group of transients with very high luminosity and short timescales of evolution, such as the so-called fast-evolving luminous transients (FELTs; e.g., Rest et al. 2018). They have a much faster rise and decline in their light curves than regular SNe. And many of them have peak luminosities much higher than normal SNe, close to the superluminous SNe (SLSNe; Quimby et al. 2011; Howell 2017). The physical origins of these FELTs are still unclear. Among them, some are characterized by a very blue color, indicating high temperature, and are also called fastrising blue optical transients (FBOTs; e.g., Drout et al. 2014; Arcavi et al. 2016).

A recently discovered extragalactic transient, AT2018cow (ATLAS18qqn), has caught much attention due to the peculiar behavior in its light curves and spectral evolution. It was discovered by ATLAS on MJD 58,285.44 (UT 2018 June 16.44; UT dates are used throughout this paper) with a magnitude of 14.76 ± 0.10 mag in the ATLAS orange band (Smartt et al. 2018). It is located far from the center of the host galaxy, CGCG 137-068 (z = 0.0141, $D_L = 63$ Mpc⁴⁰). This distance means that AT2018cow is as luminous as the peak of Type Ia SNe (SNe Ia) at discovery. As soon as this transient source was reported, astronomers from all over the world were actively conducting its follow-up observations in all bands, including ultraviolet (UV), optical, X-ray, radio, and γ ray. It was found to evolve rapidly with a rise time of less than 3 days and a peak magnitude <-20 mag. The photospheric temperature is measured to be \sim 30,000 K near the peak, and it still maintains a high temperature of \sim 15,000 K \sim 20 days after discovery (Prentice et al. 2018; Perley et al. 2019). All of these features suggest that AT2018cow can be put into the FBOTs.

The close distance makes AT2018cow the first FELT/FBOT that has well-sequenced photometric and spectroscopic observations in wave bands ranging from X-ray to radio (e.g., Prentice et al. 2018; Rivera Sandoval et al. 2018; Huang et al. 2019; Ho et al. 2019; Kuin et al. 2019; Margutti et al. 2019; Perley et al. 2019; Mohan et al. 2020), making it a rare sample for the study of FBOT-like objects. In previous studies, several possible physical mechanisms have been proposed for AT2018cow, e.g., tidal disruption of a star into an intermediate-mass black hole (Kuin et al. 2019; Perley et al. 2019, X. Li et al. 2021, in preparation), a central engine–powered SN (Prentice et al. 2018; Margutti et al. 2019), interaction of a condensed circumstellar

medium (CSM) and the SN shock (Rivera Sandoval et al. 2018; Margutti et al. 2019; Leung et al. 2020), and electron-capture collapse of a white dwarf (Lyutikov & Toonen 2019). And Margutti et al. (2019) suggested that there should be a deeply embedded X-ray source in an asymmetrical ejecta. Soker et al. (2019) proposed a common envelope jet supernova scenario for AT2018cow, where the neutron star enters the envelope of a massive star and launches jets which explode the stellar core.

In this paper, we present our optical photometric and spectroscopic observations of AT2018cow. Spectroscopic observations spanned the period from 2018 June 21 to 2018 August 14, and photometric observations lasted until 2018 September 21. In Section 2, we describe our spectroscopic and photometric observations, as well as data processing. In Section 3, we analyze the observational properties of AT2018cow, including light-curve and spectral evolution. The analysis of the host galaxy is presented in Section 4. In Section 5, we explore the possible physical origins of AT2018cow. Further discussion and a final summary are given in Sections 6 and 7, respectively.

2. Observations and Data Reduction

2.1. Photometric Observations

The optical photometric observations of AT2018cow were monitored by several observatories, including the 0.8 m Tsinghua University-NAOC telescope (TNT; Huang et al. 2012) at Xinglong Observatory of NAOC (XLT), the AZT-22 1.5 m telescope (AZT) at Maidanak Astronomical Observatory (Ehgamberdiev 2018), the telescopes of the Las Cumbres Observatory network (LCO), and the telescope of Konkoly Observatory in Hungary (KT). Photometric and spectroscopic data from LCO were obtained via the Global Supernova Project (GSP). We also collected early-time photometric data from the Observadores de Supernovas Group (ObSN) in Spain. The TNT and LCO observations were obtained in the standard Johnson-Cousins UBV bands and Sloan Digital Sky Survey (SDSS) gri bands. Long-time and short-cadenced observations in the UBVRI bands were obtained by AZT. The KT observations were obtained in the BVRI bands. Data from ObSN were obtained in the BVRI and gr bands. The entire data set covers phases from MJD 58,286.89 (2018 June 17.89) to MJD 58,348.74 (2018 August 18.74). The earliest photometric data point comes from ObSN in the V band on MJD 58,286.89, which is \sim 0.27 day earlier than that presented in Prentice et al. (2018). Besides the fast rise, the object faded very quickly. The late-time photometry may be influenced by contamination from the galaxy. Thus, for AZT, LCO, and KT, we obtained reference images in each band in 2019 March, 2018 October, and 2019 February, respectively. The reference images were obtained in all corresponding bands except for the U band of AZT. For TNT images, since the source is still bright during the observations, the influence of the background is negligible. Although the observations continued after 2018 August 18, the object became too faint to be distinguished from the background.

 $[\]overline{^{40}}$ We assume a flat universe with $H_0 = 67.7 \, \mathrm{km \ s^{-1} \ Mpc^{-1}}$, $\Omega_{\mathrm{M}} = 0.307$ (Planck Collaboration et al. 2016).

 Table 1

 Portion of Optical Photometric Observations of AT2018cow

MJD	Mag.	Mag. Error	Band	Telescope/Reference
58,285.4400	14.700	0.100	0	Smartt et al. (2018)
58,286.1950	14.320	0.010	i	Fremling (2018)
58,286.8880	13.695		V	ObSN
58,287.1130	13.593	•••	V	ObSN
58,287.1500	13.400	0.050	g	Prentice et al. (2018)
58,287.1500	13.800	0.100	r	Prentice et al. (2018)
58,287.1500	14.100	0.100	i	Prentice et al. (2018)
58,287.4440	13.674		V	ObSN
58,287.9270	13.771	•••	V	ObSN
58,287.9400	14.021	•••	I	ObSN
58,287.9460	13.926		r	ObSN
58,287.9520	13.742	•••	V	ObSN
58,287.9540	13.692		B	ObSN
58,287.9540	13.692	•••	g	ObSN
58,287.9750	13.725		R	ObSN
58,288.0677	13.809	0.021	B	LCO
58,288.0677	13.939	0.013	V	LCO
58,288.0677	13.787	0.011	g	LCO
58,288.0677	14.573	0.016	i	LCO
58,288.0677	14.295	0.017	r	LCO

(This table is available in its entirety in machine-readable form.)

All *UBVRI* and *gri* images are preprocessed using standard IRAF⁴¹ routines, which include corrections for bias, flat-fielding, and removal of cosmic rays. To remove the contamination from the host galaxy, we applied template subtraction to the AZT, LCO, and KT images. Note that the *U*-band images were not host-subtracted. The instrumental magnitudes of both AT2018cow and the reference stars were then measured using the standard point-spread function (PSF). Then, the instrumental magnitudes were converted to standard Johnson and SDSS *gri*-band magnitudes using the zero-points and color terms of each telescope. The resultant magnitudes are listed in Table 1. We also include the early photometry from Prentice et al. (2018) for comparison. The light curves are shown in Figure 1.

It can be seen that AT2018cow rises to a peak at MJD $\sim 58,287.0$ in the V, R, and I bands, where the light curves are better sampled around the peak. The latest nondetection limit is on MJD 58,284.13 in the g band (Prentice et al. 2018), so the rise time of AT2018cow is less than 2.9 days. If we take the median of the first detection (i.e., discovery by ATLAS), MJD 58,285.44, and the latest nondetection (i.e., MJD 58,284.13) as the first-light time, then the rise time is ~ 2.2 days. We apply an explosion time on MJD = $58,284.79 \pm 0.66$ throughout this paper. This rise time is too short compared to SNe, which usually have rise times of more than 10 days. After the peak, the light curves decline as fast as 0.33, 0.27, and 0.22 mag day $^{-1}$, within the first 10 days in the V, R, and I bands, respectively.

2.2. Optical Spectroscopic Observations

Our first spectrum was taken on 2018 July 21 by the 2.16 m telescope at the XLT. A total of 31 spectra were collected with different telescopes, including the XLT, the 2 m Faulkes

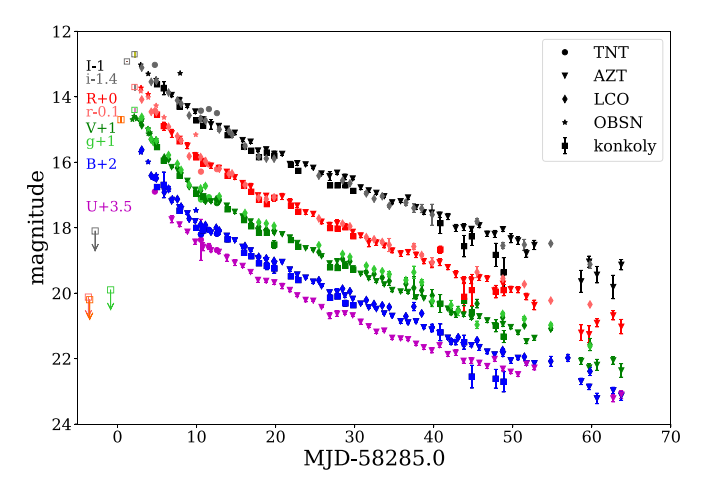


Figure 1. Light curves obtained from various telescopes. The discovery magnitude in the orange band from Smartt et al. (orange; 2018) and early follow-up photometry from Fremling (2018) and Prentice et al. (2018) are also plotted as empty squares. The prediscovery detection limits are from Fremling (2018) and Prentice et al. (2018). The magnitudes in different bands are shifted for better display.

Telescope North (FTN) of the LCO network, and the 9.2 m Hobby–Eberly Telescope (HET). The details of the spectroscopic observations are listed in Table 2.

All spectra were reduced using the standard IRAF routines, which involve corrections for bias, flat-fielding, and removal of cosmic rays. The Fe/Ar and Fe/Ne arc lamp spectra obtained during the observation nights were used to calibrate the wavelength of the spectra, and standard stars observed on the same night at similar airmasses as the SN were used to calibrate the flux of the spectra. The spectra were further corrected for continuum atmospheric extinction during flux calibration using mean extinction curves obtained at XLT and Haleakala Observatory in Hawaii. Moreover, telluric lines were removed from the spectra of XLT and FTN. We recalibrated the fluxes of the spectra to the multiband photometry data. The UV data from Perley et al. (2019) are included in the recalibration process. The recalibrated spectra are shown in Figure 2.

On 2019 September 17, when AT2018cow had already faded away in the host galaxy, a spectrum was obtained at the site of AT2018cow by HET. There are some narrow absorption lines in the resultant spectrum, which are an artifact of data reduction. The HET LRS2 is an IFU spectrograph having 280 individual fibers packed close together in a rectangular pattern with a field of view of $12'' \times 6''$, which is smaller than the size of the host galaxy of AT2018cow. Since the data reduction pipeline determines the background by combining the fibers having the lowest flux level, the background will necessarily contain some of the galaxy features. Thus, the spectra show some fake absorption lines resulting from subtraction of the emission lines from other faint parts of the host galaxy. These fake lines are manually removed from the spectrum. A detailed analysis of this spectrum is presented in Section 4.

3. Observational Properties

3.1. Light Curves and Color Evolution

The light curves of AT2018cow show much faster evolution than other optical transients. In Figure 3, we compare the *V*-band light curves of AT2018cow with other SNe of different subtypes, including the peculiar fast-evolving transient KSN2015K

⁴¹ IRAF is distributed by the National Optical Astronomy Observatories, which are operated by the Association of Universities for Research in Astronomy, Inc., under cooperative agreement with the National Science Foundation (NSF).

Table 2
Log of Optical Spectroscopy of AT2018cow

UT	MJD	Telescope	Wav. Range (Å)	Instrument	Exposure Time (s)
2018/06/21.58	58,290.58	XLT	3970-8820	BFOSC	2400
2018/06/22.32	58,291.32	HET	3640-10298	LRS2	300
2018/06/23.64	58,292.64	XLT	3970-8820	BFOSC	2400
2018/06/24.50	58,293.50	FTN	3500-10000	FLOYDS	1200
2018/06/26.30	58,295.30	HET	3640-10300	LRS2	500
2018/06/26.39	58,295.39	FTN	3500-10000	FLOYDS	1200
2018/06/26.54	58,295.54	XLT	3970-8820	BFOSC	1200
2018/06/27.57	58,296.57	XLT	3970-8820	BFOSC	2400
2018/06/28.35	58,297.35	FTN	3500-10000	FLOYDS	1200
2018/06/28.55	58,297.55	XLT	3970–8820	BFOSC	1200
2018/06/30.38	58,299.38	FTN	3500-10000	FLOYDS	1200
2018/07/01.57	58,300.57	XLT	3970-8820	BFOSC	1500
2018/07/04.48	58,303.48	FTN	3500-10000	FLOYDS	1200
2018/07/06.43	58,305.43	FTN	3500-10000	FLOYDS	2700
2018/07/08.37	58,307.37	FTN	3500-10000	FLOYDS	2700
2018/07/10.33	58,309.33	FTN	3500-10000	FLOYDS	2700
2018/07/11.41	58,310.41	FTN	3500-10000	FLOYDS	2700
2018/07/12.25	58,311.25	HET	6440-10300	LRS2	1000
2018/07/13.32	58,312.32	FTN	3500-10000	FLOYDS	2700
2018/07/14.35	58,313.35	FTN	3500-10000	FLOYDS	2700
2018/07/15.25	58,314.25	HET	3640–6970	LRS2	800
2018/07/16.31	58,315.31	FTN	3500-10000	FLOYDS	2700
2018/07/17.35	58,316.35	FTN	3500-10000	FLOYDS	2700
2018/07/19.35	58,318.35	FTN	3500-10000	FLOYDS	3600
2018/07/22.28	58,321.28	FTN	3500-10000	FLOYDS	3600
2018/07/24.34	58,323.34	FTN	3500-10000	FLOYDS	3600
2018/07/25.32	58,324.32	FTN	3500-10000	FLOYDS	3600
2018/07/26.34	58,325.34	FTN	3500-10000	FLOYDS	3600
2018/07/31.37	58,330.37	FTN	4800-10000	FLOYDS	3600
2018/08/03.25	58,333.25	FTN	3500-10000	FLOYDS	3600
2018/08/14.18	58,344.18	HET	3640-8300	LRS2	1800
2019/09/17.09	58,743.09	HET	3640-10200	LRS2	1800

(Rest et al. 2018). One can see that both the rise and decline of AT2018cow are faster than those of any other known fast-evolving SNe. The rise time is very close to that of KSN2015K, while AT2018cow is about 2 mag brighter. Most SLSNe have much slower evolution, so we do not show them in the plot. In peak luminosity, AT2018cow is close to the Type Ibn SN iPTF15ul (Hosseinzadeh et al. 2017), while it is similar to the Type Ibn SN 2006jc in terms of fast decline after the peak. It should be noted that the high luminosity and rapid evolution seen in AT 2018cow lie in the range of SNe Ibn.

During our observations, AT2018cow maintains a very blue color (i.e., $B - V \sim -0.1$ mag; Figure 4). Thus, it should suffer little reddening from its host galaxy. This can also be verified by the absence of an Na I D absorption line in the spectra. We only consider the Galactic extinction of E(B-V) = 0.08 (Schlafly & Finkbeiner 2011) for AT2018cow and ignore the host extinction in this paper. As also proposed by Perley et al. (2019), the photospheric temperature of AT2018cow is as high as ~30,000 K near maximum light and still as high as \sim 14,000 K at \sim 50 days after discovery. This is not seen in any other optical transients ever discovered. For SNe, the photospheric temperature can be high in early times but usually cools down to ~5000 K a few weeks after explosion, since the energy source is not strong enough to maintain a very high temperature. So the color of normal SNe will become red in late phases. In Figure 4, we show the B-V color evolution of AT2018cow in comparison with other SNe. The color evolution of AT2018cow resembles that of SN 2006jc.

Assuming a blackbody spectral energy distribution (SED) shape, the spectra of SN 2006jc also seem to present an unusually high effective temperature, $\sim 15,000\,\mathrm{K}$ on day 8; then the temperature grows to 25,000 K on day 25 and drops to 15,000 K around day 60. The temperature decreases to $\sim 3500\,\mathrm{K}$ and then stays flat after day 80. Nevertheless, the interaction and blending of iron lines may indeed contribute to the high temperature.

Another interesting point is that the photospheric radius seems to be decreasing since the very beginning, unlike that of normal SNe, which will increase before peak and then decrease as a result of the expansion and dilution of the ejecta. The absence of an expansion phase is the main problem of the SN origin of AT2018cow.

3.2. Spectral Evolution: Signatures of Interaction

The spectra of AT2018cow are characterized by a featureless blue continuum in the first $\sim \! 10$ days after discovery, and some broad emission features emerge later, with possible contamination from the host galaxy. Featureless and blue spectra are common in SNe due to high photospheric temperatures at early phases. Then, spectral lines appear as the temperature decreases. We create normalized spectra of AT2018cow from the observed spectra by subtracting and dividing the best-fit single-blackbody continuum of each spectrum. In the first 10 days, the spectra are characterized by a wide feature near 5000 Å, as shown in Figure 5. Later on, many broad emission

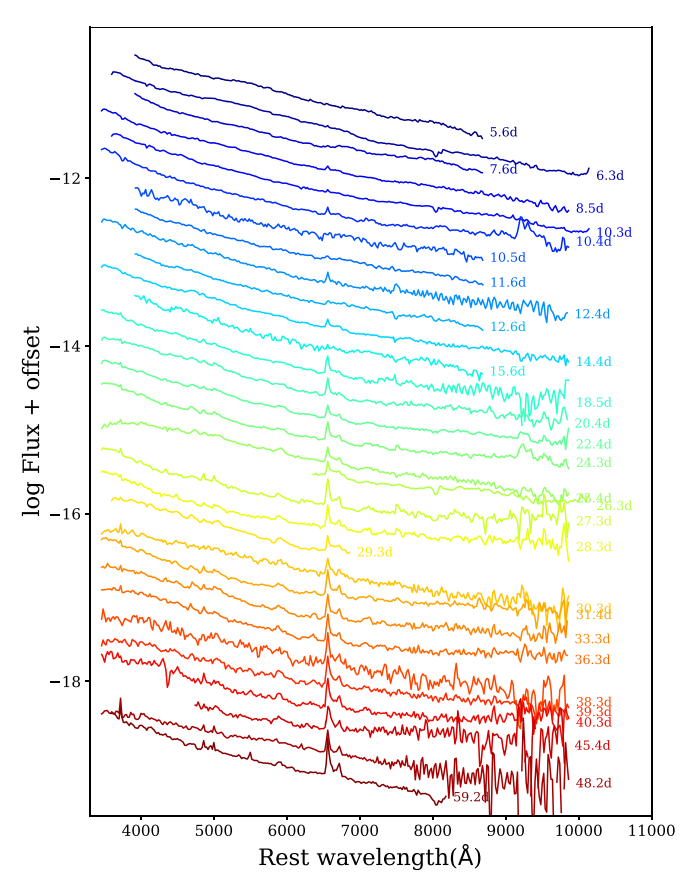


Figure 2. Optical spectra of AT2018cow. The numbers indicate days since MJD 58,285. Host galaxy emissions are not removed. The data are smoothed by a bin of 20 Å for better display.

(The data used to create this figure are available.)

lines emerge, overlapped with many narrow and strong emission lines. And there is a flux excess in the red end, which is probably due to dust emission in later phases. As proposed by Fox & Smith (2019), the spectra of AT2018cow might have shown signatures of circumstellar interaction (CSI) like SNe Ibn and IIn, while the typical features of CSI are narrow emission lines of H and He. The last spectrum taken by HET shows many narrow emission lines (FWHM $\approx 4 \text{ Å}$) that are apparently from the background host galaxy. Although other spectra of AT2018cow do show strong but broader $H\alpha$ lines since day 8 (Figure 2), it is quite possible that the lines of H are from the host galaxy, not AT2018cow. The reason is that those spectra do not have such high resolution as the HET spectrum, so the narrow lines are broadened. To figure out whether the narrow emission lines are from the host galaxy or AT2018cow, we measured the FWHMs of the H α line in each spectrum and compared it with other lines in the same spectrum. The results show that the widths of the $H\alpha$ lines are only slightly broader (by less than 10 Å, within the uncertainty) than other narrow lines, such as [N II] and [S II], indicating that they are probably from the host galaxy. Thus, we conclude that there is no significant narrow emission of H in

To better look into the spectral features of AT2018cow at t>10 days, we carefully subtracted the narrow emission lines of H α , [N II] λ 6548, 6583, and [S II] λ 6730, 6716 from the spectra. For the spectra taken from \sim 10 to \sim 59 days after

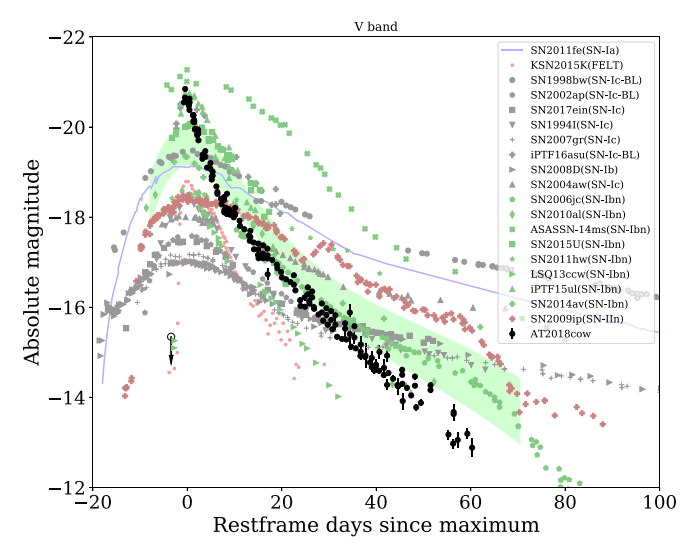
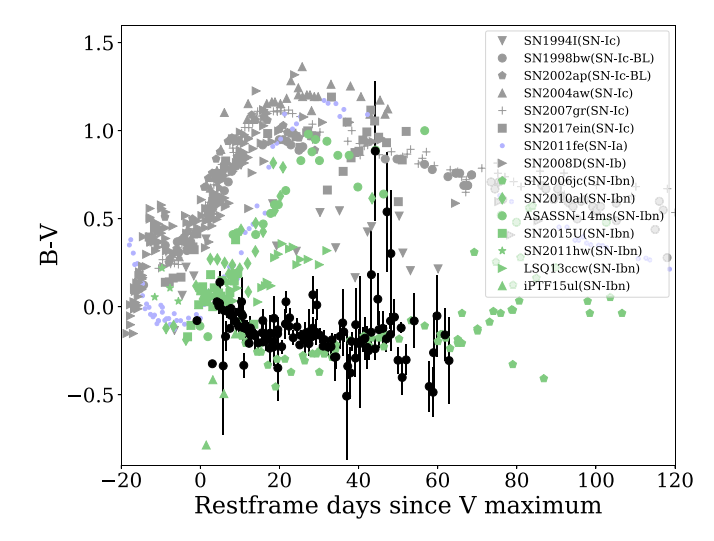


Figure 3. The V-band light curves of AT2018cow compared with other optical transients. Different colors are used to distinguish object types. The green shaded area shows the template R-band light curves of SNe Ibn from Hosseinzadeh et al. (2017). Data references: SN 2011fe (Zhang et al. 2016), KSN2015K (Rest et al. 2018), SN 1998bw (Galama et al. 1998; McKenzie & Schaefer 1999; Sollerman et al. 2000), SN 2002ap (Foley et al. 2003), SN 2017ein (Van Dyk et al. 2018; Xiang et al. 2019), SN 1994I (Yokoo et al. 1994; Richmond et al. 1996), SN 2007gr (Chen et al. 2014), iPTF16asu (Whitesides et al. 2017), SN 2008D (Mazzali et al. 2008; Modjaz et al. 2009; Bianco et al. 2014; Brown et al. 2014), SN 2004aw (Taubenberger et al. 2006), SN 2006jc (Drout et al. 2011; Bianco et al. 2014; Brown et al. 2014), SN 2010al (Brown et al. 2014; Hicken et al. 2017), ASASSN-14ms (X. F. Wang et al. 2020, in preparation), SN 2015U (Tsvetkov et al. 2015; Shivvers et al. 2016), SN 2011hw (Smith et al. 2012b; Brown et al. 2014), LSQ13ccw (Smartt et al. 2015), iPTF15ul (Hosseinzadeh et al. 2017), SN 2014av (Pastorello et al. 2016), SN 2009ip (Mauerhan et al. 2013; Smartt et al. 2015). Some of the reference data are obtained via the Open Supernova Catalog (Guillochon et al. 2017).

discovery, we identify shallow and broad emission lines that can be attributed to HI, HeI, HeII, OI, OIII, and CIII lines (as shown in Figure 6). The OI, OIII, CIII, and HeII lines dissipated after around day 45. The peaks of these lines are all slightly redshifted by up to 2000 km s⁻¹. The emission lines of AT2018cow are much broader than most SNe Ibn and IIn. The He I λ 5876 line has an FWHM of \sim 300 Å ($\nu \sim 15,000 \text{ km s}^{-1}$) at day 14, which is 1 mag higher than that of most SNe Ibn $(v \sim 1000 \,\mathrm{km \, s^{-1}})$. In late phases, the broad lines become narrower, with the FWHM decreasing to $\sim 3000 \text{ km s}^{-1}$ on day 59. Meanwhile, these broad emission lines are redshifted with velocities decreasing from $\sim 1800 \, \mathrm{km \, s^{-1}}$ when they first emerge to hundreds of kilometers per second in late phases. In the region of $H\alpha$, there is a broad emission line, which should be a blending of H α and He I λ 6678. This line is seen getting narrower over time and split into two lines after $t \sim 30 \,\mathrm{days}$, and the peaks moves to the rest wavelength. In addition to the long-existing broad emission lines, a weak and narrow (FWHM $\sim 800-1000 \,\mathrm{km \, s^{-1}}$) He I $\lambda 6678$ line emerged in the spectra after $t \sim 20$ days. This narrow line is certain to be from AT2018cow, as it does not appear in the spectrum of the host galaxy. To conclude, the broad emission lines of highly ionized elements (C III, O III) indicate that there is possible CSM interaction at very early times (t < 10 days). And the appearance of narrow He emission lines in late times (t > 20 days) implies the existence of another distant CSM formed around the progenitor object.



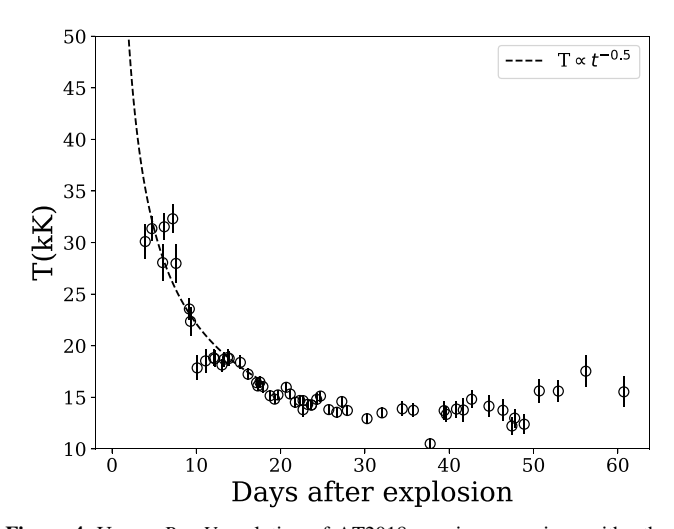


Figure 4. Upper: B - V evolution of AT2018cow, in comparison with other well-observed SNe. Symbols and references are the same as in Figure 3. Lower: temperature evolution of AT2018cow. The dashed line shows the estimation of the early temperature as $T \propto t^{-0.5}$, which is used to estimate the early-time bolometric luminosity (see Section 5).

It is natural to think of an interacting SN picture for AT2018cow. Fox & Smith (2019) found the similarity between AT2018cow and some SNe Ibn and IIn. Here we argue that although AT2018cow shows signatures of interaction similar to SNe Ibn and IIn, its spectral evolution is quite different from that of SNe Ibn and IIn. In Figure 7, we show the spectral evolution of AT2018cow compared with some well-observed SNe Ibn, SN 2006jc (Pastorello et al. 2007; Smith et al. 2008), SN 2015U (Pastorello et al. 2015b; Shivvers et al. 2016), and SN 2002ao (Pastorello et al. 2008a), and a typical SN IIn, 2010jl (Smith et al. 2012c; Zhang et al. 2012). From Figure 7, we can see the diversity of SNe Ibn. As it has weaker lines at all phases, AT2018cow seems to have different spectral features from any other interacting SNe. At earlier phases, AT2018cow is characterized by a blue featureless continuum like that seen in some core-collapse SNe (CCSNe) as a result of high temperature, i.e., SN 2015U from our comparison sample, while SN 2015U shows a narrow P Cygni absorption feature, indicating the recombination of He in the CSM (Shivvers et al. 2016). Note that the emission lines of AT2018cow emerged at later phases and are much weaker compared to SN 2006jc and SN 2002ao. Moreover, the Ca lines are very strong

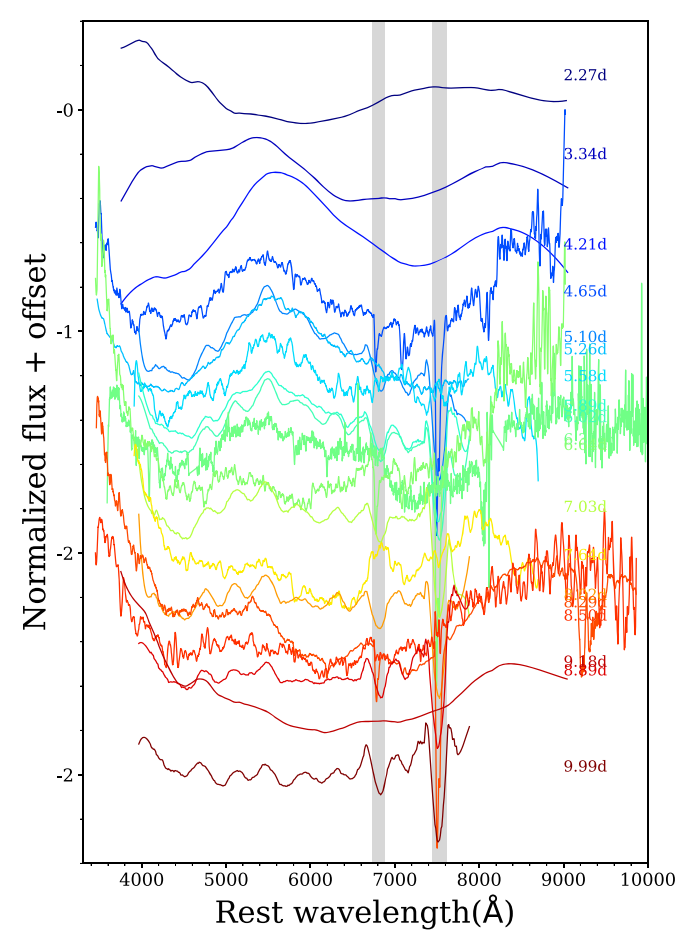


Figure 5. Normalized spectra of AT2018cow in the first 10 days. The shaded areas mark the region of telluric lines.

in SN 2006jc and SN 2015U but weak in AT2018cow. At late times, AT2018cow shows similarities to SN 2002ao, both being dominated by broad lines, while P Cygni absorption of He I lines is present in SN 2002ao, and the lines are stronger. The line velocity of He I at $t \sim +24$ days is $\sim 8500 \, \mathrm{km \, s^{-1}}$ for SN 2002ao, slightly higher than AT2018cow ($\sim 7000 \, \mathrm{km \, s^{-1}}$). Object SN 2002ao is claimed as 06jc-like, which are proposed as Wolf–Rayet (WR) stars exploded in an He-rich CSM (Pastorello et al. 2008a). Although SNe Ibn and IIn are distinguished by the strength of the H emission lines, there are some transitional objects that show roughly equal strength of the H and He emission lines, for example, SN 2005la (Pastorello et al. 2008b) and SN 2011hw (Smith et al. 2012b; Pastorello et al. 2015a).

In most interacting SNe, like SNe IIn and Ibn, the emission lines have velocities in the range of tens to a few thousand kilometers per second, depending on the wind velocities of the progenitor stars. The wind velocities are related to the type of the progenitor stars. At the same metallicities, stars with larger initial masses are expected to have stronger stellar winds and therefore higher wind velocities when they evolve to the end of life (see Smith 2014 and references therein). Some of the objects show intermediate-width emission lines (1000 km s⁻¹ < v < 4000 km s⁻¹), like SN 2006jc. In the spectra of SN 2006jc, the bluer He lines show narrow P Cygni profiles, while the redder He lines show an intermediate-width emission component (FWHM \approx 3000 km s⁻¹; Foley et al. 2007). The broad emission features in AT2018cow are apparently different from the spectral features in ordinary SNe II. The lack of absorption features implies that AT2018cow is possibly more

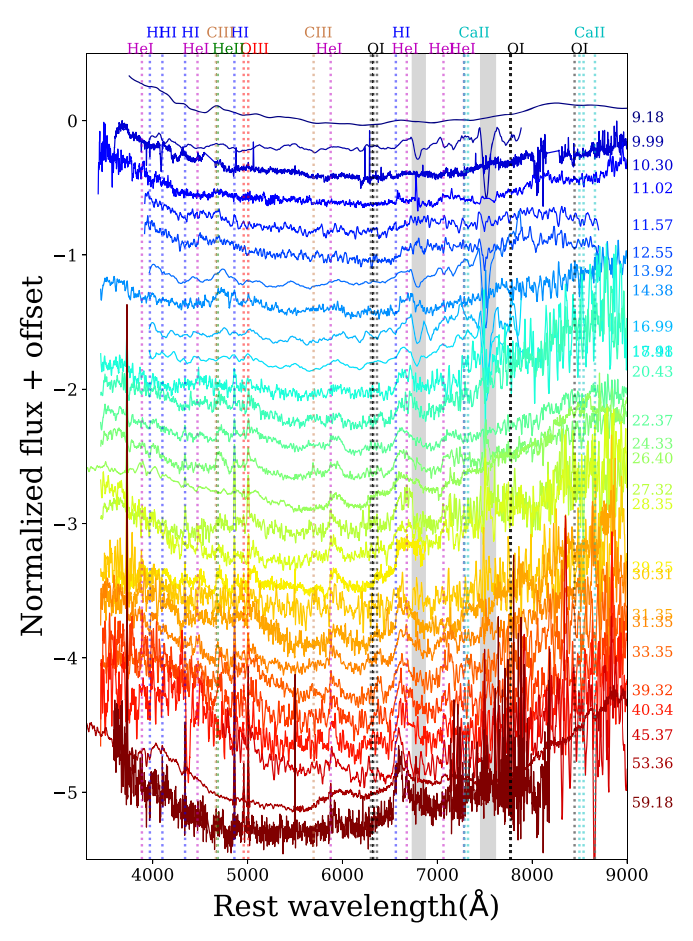


Figure 6. Normalized spectra of AT2018cow 10 days after discovery. The spectra are normalized, and the narrow emission lines from the host galaxy in the region around ${\rm H}\alpha$ in the spectra of AT2018cow are manually subtracted for better viewing. The numbers on the right mark the time in days since discovery (MJD 58,285).

similar to SNe IIn/Ibn than SNe IIP/IIL, while the velocities of the broad emission component in AT2018cow ($\nu \sim 10,000\,\mathrm{km\,s^{-1}}$) are much higher than those of normal SNe Ibn/IIn. The lack of narrow emission lines in AT2018cow and relatively weak lines make it unique among interacting SNe. This is not an argument against the interacting SN origin of AT2018cow, because spectral diversity is seen in other SNe Ibn and IIn (e.g., Hosseinzadeh et al. 2017). The absence of narrow lines might result from a closely located CSM that was immediately swept up by the shock within a short time period.

4. Host Galaxy Environment

We notice that the spectra of AT2018cow are almost featureless at early phases ($t < 10 \,\mathrm{days}$). Later on the spectra are some broader features overlapped with many narrow emission lines that are probably due to the emission from the background galaxy. We obtained a spectrum of the host at the location of AT2018cow with the 9.2 m HET on 2019 September 17 (corresponding to \sim 460 days after discovery), as shown in Figure 8.

The spectrum is characterized by that of a typical H II region, which implies that this region is currently at gas phase and star-forming. One can see strong emission lines of H, He, N, S, O, and an Na I D absorption line at the rest wavelength of the Milky Way. With this spectrum, we are able to measure the intensities

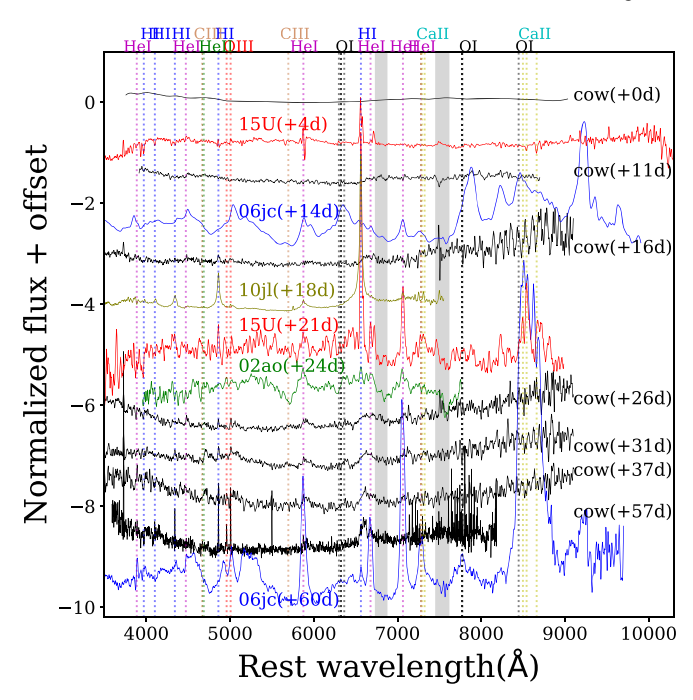
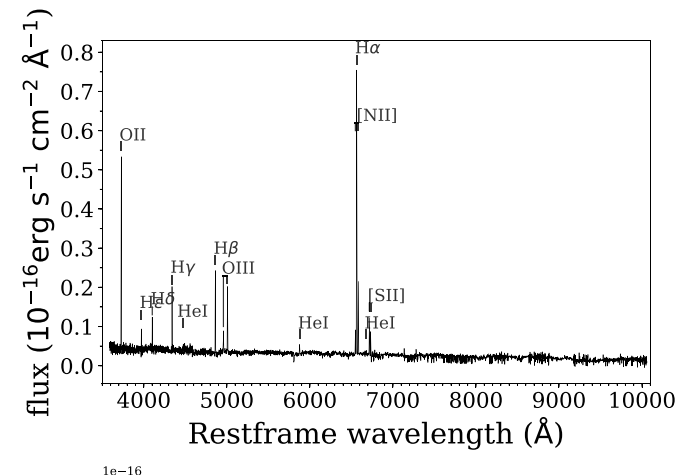


Figure 7. Normalized spectra of AT2018cow compared with other SNe. All spectra are normalized by the fitted blackbody continuum. The numbers in parentheses are the phases relative to V-band maximum; for AT2018cow, we adopt MJD 58,287. The narrow H α lines in the spectra of AT2018cow are manually subtracted for better viewing.

of the emission lines and then derive the properties of the local environment. Following Curti et al. (2017), we get a local metallicity of $12 + \log(O/H) \sim 8.65 \pm 0.07$, which is solar-like and within the range of other SNe Ibn (Pastorello et al. 2016). The star formation rate (SFR) can be derived from the luminosity of the $H\alpha$ emission line, for which we measured $L(H\alpha) \approx 1.82 \times 10^{39} \text{ erg s}^{-1}$. This is consistent with the result from Lyman et al. (2020), $L(H\alpha) \approx 1.35 \times 10^{39} \text{ erg s}^{-1}$, at the site of AT2018cow, considering that we applied a larger distance. Using the conversion factor given in Sullivan et al. (2001), we get SFR($\text{H}\alpha$)_{local} $\approx 0.015~M_{\odot}~\text{yr}^{-1}$. We also examine the [O II] $\lambda 3727$ line and get $L(\text{[O II]}) \approx 8.76 \times 10^{38}~\text{erg s}^{-1}$. With the relation given in Kennicutt (1998), we get SFR([O II])_{local} $\approx 0.012~M_{\odot}~\rm{yr}^{-1}$, which is consistent with that from the $H\alpha$ line. To get more information on the local environment of AT2018cow, we use Firefly (Wilkinson et al. 2017) to fit the spectrum with stellar population models. The input models are two M11 stellar libraries, MILES and STELIB (Maraston & Strömbäck 2011), and the initial mass function "Kroupa" (Kroupa 2001) is adopted in the fit. Figure 8 shows the best-fit spectra, from which we get a stellar mass of $M_{\star} \sim 5 \times 10^6 \, M_{\odot}$. Combining the above SFR and stellar mass information, we can get a local specific SFR (sSFR) as $\log(\text{sSFR})_{\text{local}} \sim -8.5 \, (\text{yr}^{-1}).$

The SDSS (Abolfathi et al. 2018) took one spectrum at the center of the host galaxy of AT2018cow on MJD 53,566. As the HET spectrum we obtained only provides the local information, we also use the SDSS spectrum to measure the above corresponding parameters for the whole galaxy. The resulting metallicity is the same as that measured from the HET spectrum spotted at the site of AT2018cow, while the SFR is measured as SFR($\text{H}\alpha$)_{center} $\approx 0.008~M_{\odot}~\text{yr}^{-1}$ if we do not consider any host extinction. The Firefly fit shows that the stellar mass of the nucleus is $M_{\star} \sim 2.6 \times 10^8~M_{\odot}$. We caution that the SDSS spectrum only



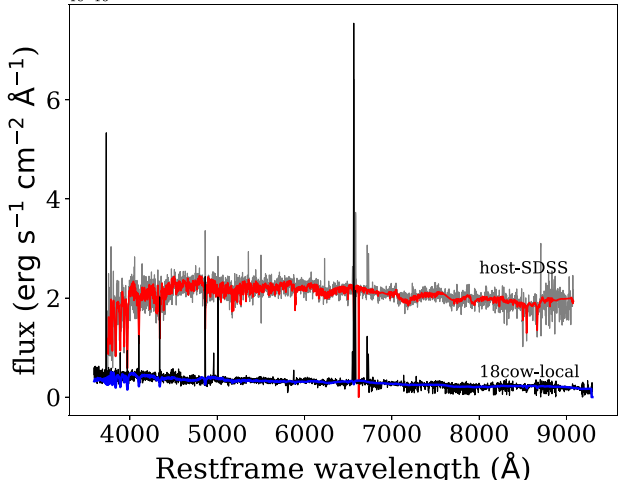


Figure 8. Upper panel: spectrum taken at the location of AT2018cow. Lower panel: Firefly fitting of the host spectra at the site of the object and galaxy center. The overplotted colored lines are the best-fit models of Firefly.

includes the flux from the galaxy center; thus, the SFR is expected to be lower. For the whole galaxy, we refer to the results from other studies. Perley et al. (2019) and Lyman et al. (2020) found the stellar mass and SFR in good agreement with each other, although they adopted different distances. At $D_L=63$ Mpc, stellar masses in these two studies become $M_\star\approx 1.56\times 10^9$ and 1.85×10^9 M_\odot , respectively. And the SFR from Lyman et al. (2020) becomes $0.20\,M_\odot$ yr⁻¹. In the following discussion, we adopt an average of these results, i.e., $M_\star\approx 1.70\times 10^9~M_\odot$, SFR $\approx 0.21\,M_\odot$ yr⁻¹, and log(sSFR) ≈ -9.88 (yr⁻¹).

The host environment may provide a clue to the physical origin of AT2018cow. We compare the host environment parameters with other well-studied transients, including SNe Ia (Smith et al. 2012a; Galbany et al. 2014), CCSNe (Svensson et al. 2010; Galbany et al. 2014), SLSNe (Angus et al. 2016), and gamma-ray bursts (GRBs; Svensson et al. 2010). As shown in Figure 9, the host galaxy of AT2018cow is located among SNe Ia, CCSNe, and GRBs but away from the SLSN group. The host galaxy of AT2018cow has a stellar mass close to the median of the GRBs but at the lower end of the SN group, except for SLSNe. We cannot say for sure which group it should belong to, and it is likely that AT2018cow is distinct from SLSNe, although AT2018cow has a peak luminosity comparable to them. Meanwhile, the local high SFR of AT2018cow may imply that AT2018cow probably originated from a massive star.

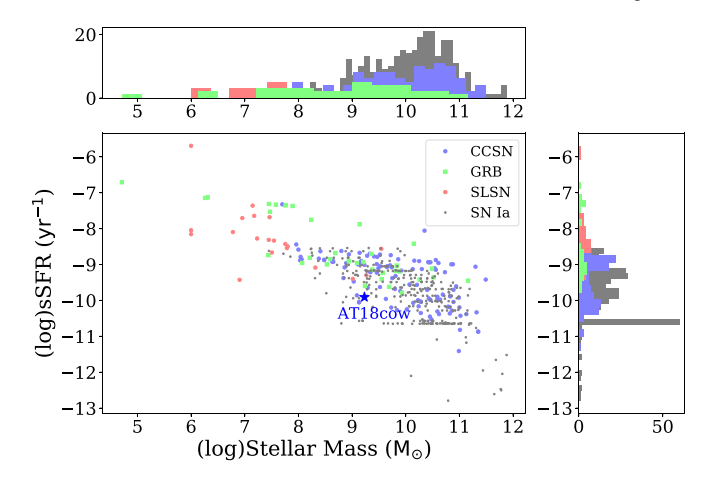


Figure 9. Host galaxy parameters of AT2018cow compared with other types of transients.

5. Modeling the Rapidly Evolving Light Curves

The physical interpretation of AT2018cow is still in debate, although there are already several papers trying to uncover its physical origin. The radioactive decay (RD) of ⁵⁶Ni is a wellknown energy source for SNe (Arnett 1982). The bolometric light curve of AT2018cow cannot be powered by pure ⁵⁶Ni, as the peak luminosity would require an ejected ⁵⁶Ni mass of $\sim 6 \, M_{\odot}$ but a low ejecta mass $< 1 \, M_{\odot}$. In the above analysis, we find a high resemblance of the light curves of AT2018cow to those of SNe Ibn, and signatures of CSI are found in the spectra, so we try to fit the light curves of AT2018cow using the CSI model. The fast-declining and luminous bolometric light curve of SN 2006jc has been successfully modeled by CSI models (e.g., Tominaga et al. 2008; Chugai 2009). The rapidly declining light curves can be related to the early shock cooling from the progenitor envelope. Since the progenitor has lost most of its hydrogen envelope, the shock cooling should be weak and short for the core collapse of a massive star. Another reasonable interpretation is the interaction of the SN ejecta with the surrounding CSM. This can be supported by the emission lines in the spectra (see Section 3.2).

We construct the bolometric light curves by integrating the UV and optical flux (the UV data are taken from Perley et al. 2019) and then apply a model in which CSI is dominating the early-time light curve. In order to better constrain the fitting, especially to obtain data before the peak, we estimate the prepeak bolometric luminosities based on the following assumptions: (1) the SED of AT2018cow is a blackbody and (2) the photometric temperature evolves as a power law $T \propto (t - t_0)^{-0.5}$, as we derived from the early temperature evolution. Then, the bolometric luminosities before MJD 58,288.44 are estimated using the single-band photometry data. We adopt a hybrid model that includes ⁵⁶Ni powering and the interaction of the SN ejecta with a dense CSM with a density profile as a power law, i.e., $\rho_{\rm CSM} \propto r^{-s}$, where the typical value of s is 2 and 0 (e.g., Chatzopoulos et al. 2012, 2013; Wang et al. 2019). In our model, the density distribution of the ejecta is uniform in the inner region ($\delta = 0$) and follows a power law $(\rho \propto r^{-12})$ in the outer region. The early fast-rising light curve of AT2018cow is mainly powered by CSI, while the slower-declining tail is dominated by RD of 56 Ni. We first consider the case of s = 2, which corresponds to a steady-wind CSM. The best-fit light curve is shown in Figure 10, and the fitted parameters are presented in Table 3. As shown in Figure 10, our CSI+RD(s=2) model can fit the observations quite well. The mass-loss rate of the

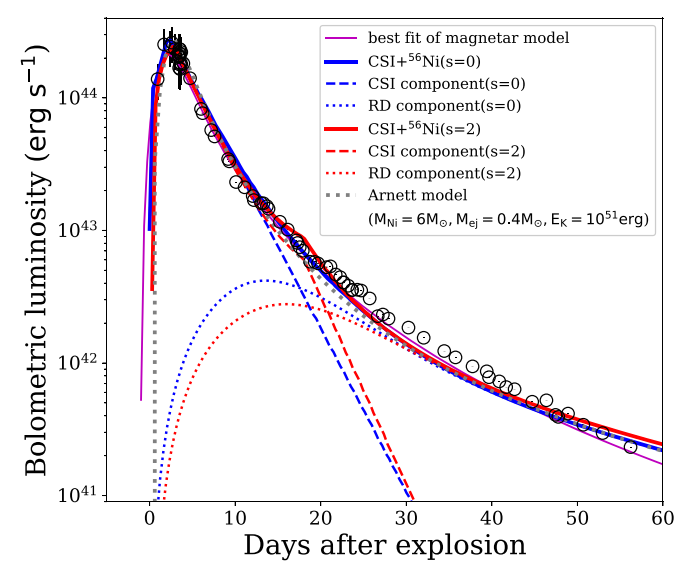


Figure 10. Bolometric light curve of AT2018cow. Best-fit models of CSI+RD with s=0 and 2 are plotted with blue and red solid lines, respectively. The two components of the models are shown by dashed (CSI) and dotted (RD) lines, respectively. The best-fit magnetar model is plotted as a magenta solid line. A pure RD model is also shown by a gray dotted line as a reference.

progenitor star can be estimated as $0.1(v_{\rm CSM}/100~{\rm km~s}^{-1})~M_{\odot}~{\rm yr}^{-1}$, $\sim 1~M_{\odot}~{\rm yr}^{-1}$ with $v_{\rm CSM}\sim 1000~{\rm km~s}^{-1}$. Margutti et al. (2019) also reached a similar conclusion by analyzing the optical and X-ray data. Such a mass-loss rate is much higher than that found from the radio observations of AT2018cow ($\dot{M}\sim 10^{-4}-10^{-3}~M_{\odot}~{\rm yr}^{-1}$; Ho et al. 2019 had a similar conclusion). If we set a limit on the massloss rate, the model can hardly fit the observations. Thus, we claim that the early bright and fast-evolving light curve of AT2018cow cannot be produced by CSI with a steady stellar wind.

We then try the other case where s = 0, i.e., the density of the CSM is a constant. The fitting result is shown in Figure 10, and the fitted parameters are presented in Table 3. As shown in Figure 10, with $M_{\rm ej} \approx 3.16~M_{\odot}$, $M_{\rm CSM} \approx 0.04~M_{\odot}$, and $M_{\rm Ni} \approx 0.23~M_{\odot}$, the CSM+ 56 Ni(s=0) model can also provide a plausible fit for the observed bolometric light curve. The inferred inner radius of the CSM gives a constraint on the radius of the progenitor star $R < 3 R_{\odot}$, which is consistent with the typical size of WR stars. The CSM shell extends outward to a radius of 8.70×10^{13} cm (\approx 1200 R_{\odot}), implying that the CSM was formed shortly before the explosion. Such a CSM shell can be produced by an episodic mass ejection from the progenitor star, like a luminous blue variable (LBV), or from a common-envelope episode of a binary system. Combining the mass and velocity of the ejecta, the kinetic energy of the ejecta can be estimated as 6.6×10^{51} erg, several times higher than that of the ordinary SNe Ibc and rather similar to the broad-lined SNe Ic (SNe Ic-BL; Lyman et al. 2016), which are found to be possibly associated with long GRBs (e.g., SN 1998bw; Iwamoto et al. 1998; Nakamura et al. 2001). The high velocity of the ejecta might be connected to a relativistic jet.

Alternatively, the bolometric luminosity and effective temperature evolution can be explained by a magnetar-powered model (Nicholl et al. 2017). Assuming that the opacities of the ejecta are $\kappa=0.2~{\rm cm^2~g^{-1}}$ for the optical photon and $\kappa_{\rm mag}=0.013~{\rm cm^2~g^{-1}}$ for the magnetar wind, respectively, the best-fit parameters for this model are $t_0=58,283.4,~M_{\rm ej}=0.1~M_{\odot},~v_{\rm ej}=2.72\times10^4~{\rm km~s^{-1}},~P=4.5~{\rm ms},~{\rm and}~B=1.11\times10^{14}~{\rm G},~{\rm where}~P~{\rm and}~B~{\rm are}$ the initial spin period and magnetic field strength of the nascent magnetar, respectively. We caution that the best-fit $M_{\rm ej}=0.1~M_{\odot}$ is the

	s = 0	s = 2
t_0	MJD 58,284.5	MJD 58,284.7
$M_{\rm ej}~(M_{\odot})$	3.16	1.69
$M_{\rm ej} (M_{\odot})$ $x_0^{\rm a}$	0.63	0.76
$v_{\rm ej}~({\rm km~s^{-1}})$	26,000	13,600
$M_{\mathrm{Ni}} (M_{\odot})$	0.23	0.14
$M_{\mathrm{CSM}} \ (M_{\odot})$	0.04	0.12
$r_{\rm CSM,in} \ ({\rm cm})^{\rm b}$	2.11×10^{11}	1.03×10^{13}
$r_{\rm CSM,out} {\rm (cm)}^{\rm c}$	8.70×10^{13}	3.16×10^{14}
$\rho_{\rm CSM,in}~({\rm g~cm}^{-3})^{\rm d}$	2.9×10^{-11}	5.6×10^{-10}
$\epsilon^{\mathbf{e}}$	0.22	0.65
κ	0.14	0.15
κ_{γ}	0.015	0.014

Notes.

lower limit of the magnetar model in our fitting program. If no limit is given, the fitting tends to find a significantly lower value to fit the narrow light curve better. This may imply that the magnetar-powered model requires a rather low ejecta mass for AT2018cow.

6. Discussion: Progenitor Properties

In the previous section, we analyzed the bolometric light curve of AT2018cow based on the assumption that it is of SN origin. While we do not rule out other possibilities, especially a TDE origin, a main problem of the SN origin for AT2018cow is that the process of an expanding photosphere is missing. In early phases, the photospheric velocity may be very high (~0.1c) for AT2018cow in the early phases. The photospheric radius has kept decreasing since very early times. This can be a clue for interpreting AT2018cow as a TDE. Both Margutti et al. (2019) and Lyman et al. (2020) found no evidence of the connection between the site of AT2018cow and an intermediate-mass black hole. Nevertheless, one can notice that the measurements of the photospheric radius start after the peak, probably suggesting that the expanding phase is not observed.

The magnetar-powered model can make a good fit to the bolometric light curve. The best-fit B and P of the central engine lies in the range of SLSNe (Lin et al. 2020 and references therein). The distinction between AT2018cow and SLSNe is the evolution timescale, which is related to the ejecta mass. Nicholl et al. (2017) found $M_{\rm ej} \geqslant 2.2~M_{\odot}$ with an average of 4.8 M_{\odot} . Besides, the low ejected mass ($M_{\rm ej} \sim 0.1~M_{\odot}$) required by the magnetar model for AT2018cow is not likely favorable for a massive star, except for some really extreme cases. Some studies find that massive stars can be ultrastripped by binary interaction with a compact neutron star (Tauris et al. 2015). But in these cases, little H or He remains in the progenitor system, which is not consistent with the observed spectral features of AT2018cow. Thus, we disfavor the magnetar model for AT2018cow.

Our CSI+RD(s=0) model makes a plausible fit to the bolometric light curve of AT2018cow. With R < 3 R_{\odot} , the

^a The dimensionless radius of the division between the inner and outer regions of the ejecta.

^b The inner radius of CSM.

^c The outer radius of CSM.

 $^{^{\}rm d}$ The CSM density at $r_{\rm CSM,in}$.

^e The radiation efficiency.

progenitor star is most likely to be a compact WR star. The ejected mass $(M_{\rm ej} \approx 3~M_{\odot})$ is lower than that predicted by single stellar evolution models (e.g., Georgy et al. 2012) but around the mean value of SNe Ibc (Lyman et al. 2016). This might be a result of binary interaction or episodic eruptive mass loss during the lifetime of massive stars. It is hard to derive the mass of the progenitor star simply from the ejecta mass, since the mass-loss mechanisms of massive stars can be complicated and ambiguous.

In the case of s = 0, the CSM can be dense shells formed by the strong stellar winds of WR stars or an eruptive of LBV stars (Chevalier & Liang 1989; Dwarkadas 2011). According to our fitting result, with a wind velocity of $100 \, \mathrm{km \, s^{-1}}$, the eruption started several months before core collapse and was possibly still on when exploding. The average mass-loss rate is $\sim 0.15 \, M_{\odot} \, \mathrm{yr}^{-1}$, or even higher if the wind velocity is higher, lying well in the range of LBV eruptions (Smith 2014). Such mass-loss behavior can be found in some SNe IIn and Ibn (Gal-Yam et al. 2007; Kiewe et al. 2012; Moriya et al. 2014a; Pastorello et al. 2015a; Taddia et al. 2015). Under this scenario, the progenitor of AT2018cow might be a massive star that is in an eruptive state. However, with R < 3 R_{\odot} , the progenitor star is most likely to be H- or even He-poor, and so is the CSM. There is a possibility that H and He are mixed into the inner shells so that the progenitor can keep some H/He at core collapse.

Meanwhile, binary interaction might dominate the evolution of massive stars, which are thought to be the progenitors of stripped-envelope SNe. Mass loss can be quite efficient in binaries (Eldridge et al. 2017). Object SN 2006jc is a representative of interacting SNe originating from binary massive stars (Maund et al. 2016; Sun et al. 2020). In the binary scenario, the progenitors can be less massive stars, and the companion stars evolve slower so that they can keep their H/He envelopes. A common-envelope episode of a binary system can also form this dense CSM shell. The detection of H and He lines in the spectra of AT2018cow indicates that the CSM is not H-free. So it is quite possible that the CSM is from the companion star rather than the progenitor itself. The slightly redshifted peaks of the emission lines in the spectra of AT2018cow suggest asymmetry of the CSM, in favor of the common-envelope picture.

The progenitor star could be a very massive star that has experienced violent mass loss due to pulsational ejection. Recently, Leung et al. (2020) proposed a scenario based on a pulsational pair-instability SN model, concluding that the rapidly evolving light curve of AT2018cow can be explained by a $42 M_{\odot}$ He star exploding in a dense He-rich CSM ($M_{\rm CSM} \sim 0.5 \, M_{\odot}$). The proposed model can fit the bolometric light curve well (at t <30 days). However, the presence of H lines in the spectra of AT2018cow is inconsistent with the assumption that both the ejecta and CSM formed around AT2018cow should be H-poor. Leung et al. (2020) tested different compositions of the CSM and found that the amount of H in the CSM only has a slight effect on the bolometric light curve. Our fitting result is in agreement with Leung et al. (2020) in terms of the density and size of the CSM, but we find a much lower CSM mass. We do not assume any Ni mixing, while Leung et al. (2020) assumes that Ni is fully mixed into the outer layers of the ejecta. Nevertheless, both models may be plausible. Our model can correspond to a massive progenitor in a binary system, while Leung et al. (2020) required a very massive star whose zero-age main-sequence (ZAMS) mass is $80 M_{\odot}$. It is worth noting that Leung et al. (2019) claimed that a massive He

core can only be formed under low metallicity ($Z \le 0.5 \ Z_{\odot}$), which is inconsistent with our measurement of a solar-like metallicity environment for the progenitor of AT2018cow (see Section 4). This may imply that the progenitor of AT2018cow did not undergo pulsational pair instability (PPI).

The fast-evolving light curves of AT2018cow may be related to a very low ejecta mass, which is consistent with electroncapture SNe (ECSNe; Nomoto 1984, 1987; Nomoto & Kondo 1991; Moriya et al. 2014b). Stars with a ZAMS mass of $\sim 8-12~M_{\odot}$ form degenerate cores of O, Ne, and Mg, which are susceptible to electron capture, leading to core collapse. For KSN 2015K, an example of a FELT, Rest et al. (2018) preferred a CSI model, while Tolstov et al. (2019) found that the collapse of an ONeMg star surrounded by an optically thick CSM can also explain the fast rise of the light curve. However, the progenitors of ECSNe are thought to be super–asymptotic giant branch stars, which have stellar winds with relatively low velocities ($\sim 10 \text{ km s}^{-1}$). According to theoretical predictions, ECSNe are usually faint and have low explosion energies (e.g., Botticella et al. 2009; Kawabata et al. 2010; Hiramatsu et al. 2020). Thus, the ECSN scenario is unlikely for AT2018cow.

7. Summary

In this paper, we present our photometric and spectroscopic observations of the peculiar transient AT2018cow. The multiband photometry covers from peak to \sim 70 days, and the spectroscopy ranges from 5 to \sim 50 days after discovery. The rapid rise ($t_r \leq$ 2.9 days), luminous light curves ($M_{V,\mathrm{peak}} \sim -20.8\,\mathrm{mag}$), and fast postpeak decline make AT2018cow stand out from any other optical transients. After a thorough analysis, we find that the light curves and color evolution show a high resemblance to some SNe Ibn. With a detailed analysis of the spectral evolution and line identifications, we find that AT2018cow shows similar properties to the interacting SNe, like SNe IIn and Ibn. Some broad emission lines due to H I, He I, He II, C III, O I, and O III emerge at $t \sim$ 10 days, with $v_{\rm FWHM}$ decreasing from \sim 11,000 to \sim 3000 km s⁻¹ at the end of our observations. At $t \sim 20$ days, narrow and weak He I lines ($v_{\rm FWHM} \sim 800{\text -}1000~{\rm km~s}^{-1}$) are overlaid on the broad lines. These emission lines are evidence of interaction between the ejecta and an H-rich CSM. Furthermore, we spotted the site of AT2018cow after it faded away and found that it has a solar-like metallicity. The host galaxy of AT2018cow has properties similar to those of GRBs and CCSNe but is distinct from SLSNe and SNe Ia. A high SFR at the site of AT2018cow implies that AT2018cow might originate from a massive star.

Based on the interpretation of a CSI SN, we fit the bolometric light curves with CSI+RD models. We find that in order to produce the fast and bright early light curve of AT2018cow, the CSI model with a steady wind requires a much larger mass-loss rate than that derived from radio observations. With a dense uniform CSM shell, the CSI+RD model can make a plausible fit with the best-fit parameters $M_{\rm ej} \sim 3.16~M_{\odot}$, $M_{\rm CSM} \sim 0.04~M_{\odot}$, and $M_{\rm Ni} \sim 0.23~M_{\odot}$. Such a CSM shell can be formed by eruptive mass ejection of LBVs immediately before core collapse or common-envelope ejection in binaries. With $Z \approx Z_{\odot}$, the progenitor is less likely to have undergone PPI. We conclude that the progenitor of AT2018cow is likely to be a less massive star in a binary system.

We acknowledge the support of the staff of the Xinglong 2.16 m and Lijiang 2.4 m telescopes. This work is supported by the National Natural Science Foundation of China (NSFC

grants 12033003, 11761141001, and 11633002) and the National Program on Key Research and Development Project (grant No. 2016YFA0400803). This work was also partially supported by the Open Project Program of the Key Laboratory of Optical Astronomy, National Astronomical Observatories, Chinese Academy of Sciences. This work is partially supported by the Scholar Program of Beijing Academy of Science and Technology (DZ:BS202002). J.J.Z. is supported by the National Science Foundation of China (NSFC, grants 11403096 and 11773067), the Key Research Program of the CAS (grant No. KJZD-EW-M06), the Youth Innovation Promotion Association of the CAS (grant 2018081), and the CAS "Light of West China" Program. X.L. was supported by the China Postdoctoral Science Foundation funded project (No. 2017m610866). This work makes use of the LCO network. J.B., D.A.H., and D.H. were supported by NSF grant AST-1911225 and NASA grant 80NSSC19kf1639. Research by S.V. is supported by NSF grants AST-C1813176 and AST-2008108. We thank the staff of the AZT for their observations and allowance of the use of the data.

J.V. and his group at Konkoly Observatory are supported by the project "Transient Astrophysical Objects" GINOP 2.3.2-15-2016-00033 of the National Research, Development and Innovation Office (NKFIH), Hungary, funded by the European Union. L.K. received support from Hungarian National Research, Development and Innovation Office grant OTKA K-131508 and the János Bolyai Research Scholarship of the Hungarian Academy of Sciences. A.B. has been supported by the Lendület Program of the Hungarian Academy of Sciences, project No. LP2018-7/2019. Zs.B. acknowledges the support provided by the Hungarian National Research, Development and Innovation Office (NKFIH), project No. PD-123910, and the support of the János Bolyai Research Scholarship of the Hungarian Academy of Sciences.

Software: ZrutyPhot (J. Mo et al. 2021, in preparation), IRAF (Tody 1993, 1986), Firefly (Wilkinson et al. 2017).

ORCID iDs

```
Danfeng Xiang https://orcid.org/0000-0002-1089-1519
Xiaofeng Wang https://orcid.org/0000-0002-7334-2357
Jamison Burke https://orcid.org/0000-0003-0035-6659
Daichi Hiramatsu  https://orcid.org/0000-0002-1125-9187
Griffin Hosseinzadeh https://orcid.org/0000-0002-0832-2974
Curtis McCully https://orcid.org/0000-0001-5807-7893
Stefan Valenti https://orcid.org/0000-0001-8818-0795
József Vinkó https://orcid.org/0000-0001-8764-7832
J. Craig Wheeler https://orcid.org/0000-0003-1349-6538
Davron Mirzaqulov https://orcid.org/0000-0003-0570-6531
Attila Bódi  https://orcid.org/0000-0002-8585-4544
Zsófia Bognár https://orcid.org/0000-0002-8493-9781
Ottó Hanyecz https://orcid.org/0000-0002-9415-5219
András Pál https://orcid.org/0000-0001-5449-2467
Krisztián Sárneczky https://orcid.org/0000-0003-0926-3950
Bálint Seli  https://orcid.org/0000-0002-3658-2175
Róbert Szakáts https://orcid.org/0000-0002-1698-605X
Tianmeng Zhang https://orcid.org/0000-0002-8531-5161
Jujia Zhang https://orcid.org/0000-0002-8296-2590
```

References

```
Abolfathi, B., Aguado, D. S., Aguilar, G., et al. 2018, ApJS, 235, 42
Angus, C. R., Levan, A. J., Perley, D. A., et al. 2016, MNRAS, 458, 84
```

```
Arcavi, I., Wolf, W. M., Howell, D. A., et al. 2016, ApJ, 819, 35
Arnett, W. D. 1982, ApJ, 253, 785
Bianco, F. B., Modjaz, M., Hicken, M., et al. 2014, ApJS, 213, 19
Botticella, M. T., Pastorello, A., Smartt, S. J., et al. 2009, MNRAS, 398, 1041
Brown, P. J., Breeveld, A. A., Holland, S., Kuin, P., & Pritchard, T. 2014,
Chatzopoulos, E., Wheeler, J. C., & Vinko, J. 2012, ApJ, 746, 121
Chatzopoulos, E., Wheeler, J. C., Vinko, J., Horvath, Z. L., & Nagy, A. 2013,
   ApJ, 773, 76
Chen, J., Wang, X., Ganeshalingam, M., et al. 2014, ApJ, 790, 120
Chevalier, R. A., & Liang, E. P. 1989, ApJ, 344, 332
Chugai, N. N. 2009, MNRAS, 400, 866
Curti, M., Cresci, G., Mannucci, F., et al. 2017, MNRAS, 465, 1384
Drout, M. R., Chornock, R., Soderberg, A. M., et al. 2014, ApJ, 794, 23
Drout, M. R., Soderberg, A. M., Gal-Yam, A., et al. 2011, ApJ, 741, 97
Dwarkadas, V. V. 2011, MNRAS, 412, 1639
Ehgamberdiev, S. 2018, NatAs, 2, 349
Eldridge, J. J., Stanway, E. R., Xiao, L., et al. 2017, PASA, 34, e058
Foley, R. J., Papenkova, M. S., Swift, B. J., et al. 2003, PASP, 115, 1220
Foley, R. J., Smith, N., Ganeshalingam, M., et al. 2007, ApJL, 657, L105
Fox, O. D., & Smith, N. 2019, MNRAS, 488, 3772
Fremling, C. 2018, ATel, 11738, 1
Galama, T. J., Vreeswijk, P. M., van Paradijs, J., et al. 1998, Natur, 395, 670
Galbany, L., Stanishev, V., Mourão, A. M., et al. 2014, A&A, 572, A38
Gal-Yam, A., Leonard, D. C., Fox, D. B., et al. 2007, ApJ, 656, 372
Georgy, C., Ekström, S., Meynet, G., et al. 2012, A&A, 542, A29
Guillochon, J., Parrent, J., Kelley, L. Z., & Margutti, R. 2017, ApJ, 835, 64
Hicken, M., Friedman, A. S., Blondin, S., et al. 2017, ApJS, 233, 6
Hiramatsu, D., Howell, D. A., Van Dyk, S. D., et al. 2020, arXiv:2011.02176
Ho, A. Y. Q., Phinney, E. S., Ravi, V., et al. 2019, ApJ, 871, 73
Hosseinzadeh, G., Arcavi, I., Valenti, S., et al. 2017, ApJ, 836, 158
Howell, D. A. 2017, in Superluminous Supernovae, ed. A. W. Alsabti &
   P. Murdin (Berlin: Springer), 431
Huang, F., Li, J.-Z., Wang, X.-F., et al. 2012, RAA, 12, 1585
Huang, K., Shimoda, J., Urata, Y., et al. 2019, ApJL, 878, L25
Iwamoto, K., Mazzali, P. A., Nomoto, K., et al. 1998, Natur, 395, 672
Kawabata, K. S., Maeda, K., Nomoto, K., et al. 2010, Natur, 465, 326
Kennicutt, R. C. J. 1998, ARA&A, 36, 189
Kiewe, M., Gal-Yam, A., Arcavi, I., et al. 2012, ApJ, 744, 10
Kroupa, P. 2001, MNRAS, 322, 231
Kuin, N. P. M., Wu, K., Oates, S., et al. 2019, MNRAS, 487, 2505
Leung, S.-C., Blinnikov, S., Nomoto, K., et al. 2020, ApJ, 903, 66
Leung, S.-C., Nomoto, K., & Blinnikov, S. 2019, ApJ, 887, 72
Lin, W. L., Wang, X. F., Wang, L. J., & Dai, Z. G. 2020, ApJL, 903, L24
Lyman, J. D., Bersier, D., James, P. A., et al. 2016, MNRAS, 457, 328
Lyman, J. D., Galbany, L., Sánchez, S. F., et al. 2020, MNRAS, 495, 992
Lyutikov, M., & Toonen, S. 2019, MNRAS, 487, 5618
Maraston, C., & Strömbäck, G. 2011, MNRAS, 418, 2785
Margutti, R., Metzger, B. D., Chornock, R., et al. 2019, ApJ, 872, 18
Mauerhan, J. C., Smith, N., Filippenko, A. V., et al. 2013, MNRAS, 430,
Maund, J. R., Pastorello, A., Mattila, S., Itagaki, K., & Boles, T. 2016, ApJ,
   833, 128
Mazzali, P. A., Valenti, S., Della Valle, M., et al. 2008, Sci, 321, 1185
McKenzie, E. H., & Schaefer, B. E. 1999, PASP, 111, 964
Modjaz, M., Li, W., Butler, N., et al. 2009, ApJ, 702, 226
Mohan, P., An, T., & Yang, J. 2020, ApJL, 888, L24
Moriya, T. J., Maeda, K., Taddia, F., et al. 2014a, MNRAS, 439, 2917
Moriya, T. J., Tominaga, N., Langer, N., et al. 2014b, A&A, 569, A57
Nakamura, T., Mazzali, P. A., Nomoto, K., & Iwamoto, K. 2001, ApJ,
   550, 991
Nicholl, M., Guillochon, J., & Berger, E. 2017, ApJ, 850, 55
Nomoto, K. 1984, ApJ, 277, 791
Nomoto, K. 1987, ApJ, 322, 206
Nomoto, K., & Kondo, Y. 1991, ApJL, 367, L19
Pastorello, A., Benetti, S., Brown, P. J., et al. 2015a, MNRAS, 449, 1921
Pastorello, A., Mattila, S., Zampieri, L., et al. 2008a, MNRAS, 389, 113
Pastorello, A., Quimby, R. M., Smartt, S. J., et al. 2008b, MNRAS, 389, 131
Pastorello, A., Smartt, S. J., Mattila, S., et al. 2007, Natur, 447, 829
Pastorello, A., Tartaglia, L., Elias-Rosa, N., et al. 2015b, MNRAS, 454, 4293
Pastorello, A., Wang, X. F., Ciabattari, F., et al. 2016, MNRAS, 456, 853
Perley, D. A., Mazzali, P. A., Yan, L., et al. 2019, MNRAS, 484, 1031
Planck Collaboration, Ade, P. A. R., Aghanim, N., et al. 2016, A&A, 594, A13
Prentice, S. J., Maguire, K., Smartt, S. J., et al. 2018, ApJL, 865, L3
Quimby, R. M., Kulkarni, S. R., Kasliwal, M. M., et al. 2011, Natur, 474, 487
Rest, A., Garnavich, P. M., Khatami, D., et al. 2018, NatAs, 2, 307
```

```
Richmond, M. W., van Dyk, S. D., Ho, W., et al. 1996, AJ, 111, 327
Rivera Sandoval, L E, Maccarone, T J, Corsi, A, et al. 2018, MNRAS,
   480, L146
Schlafly, E. F., & Finkbeiner, D. P. 2011, ApJ, 737, 103
Shivvers, I., Zheng, W. K., Mauerhan, J., et al. 2016, MNRAS, 461, 3057
Smartt, S. J., Clark, P., Smith, K. W., et al. 2018, ATel, 11727, 1
Smartt, S. J., Valenti, S., Fraser, M., et al. 2015, A&A, 579, A40
Smith, M., Nichol, R. C., Dilday, B., et al. 2012a, ApJ, 755, 61
Smith, N. 2014, ARA&A, 52, 487
Smith, N., Foley, R. J., & Filippenko, A. V. 2008, ApJ, 680, 568
Smith, N., Mauerhan, J. C., Silverman, J. M., et al. 2012b, MNRAS, 426, 1905
Smith, N., Silverman, J. M., Filippenko, A. V., et al. 2012c, AJ, 143, 17
Soker, N., Grichener, A., & Gilkis, A. 2019, MNRAS, 484, 4972
Sollerman, J., Kozma, C., Fransson, C., et al. 2000, ApJL, 537, L127
Sullivan, M., Mobasher, B., Chan, B., et al. 2001, ApJ, 558, 72
Sun, N.-C., Maund, J. R., Hirai, R., Crowther, P. A., & Podsiadlowski, P. 2020,
  MNRAS, 491, 6000
Svensson, K. M., Levan, A. J., Tanvir, N. R., Fruchter, A. S., & Strolger, L. G.
   2010, MNRAS, 405, 57
Taddia, F., Sollerman, J., Fremling, C., et al. 2015, A&A, 580, A131
```

```
Taubenberger, S., Pastorello, A., Mazzali, P. A., et al. 2006, MNRAS,
  371, 1459
Tauris, T. M., Langer, N., & Podsiadlowski, P. 2015, MNRAS, 451, 2123
Tody, D. 1986, Proc. SPIE, 627, 733
Tody, D. 1993, in ASP Conf. Ser. 52, Astronomical Data Analysis Software
  and Systems II, ed. R. J. Hanisch, R. J. V. Brissenden, & J. Barnes (San
  Francisco, CA: ASP), 173
Tolstov, A., Nomoto, K., Sorokina, E., et al. 2019, ApJ, 881, 35
Tominaga, N., Limongi, M., Suzuki, T., et al. 2008, ApJ, 687, 1208
Tsvetkov, D. Y., Volkov, I. M., & Pavlyuk, N. N. 2015, IBVS, 6140, 1
Van Dyk, S. D., Zheng, W., Brink, T. G., et al. 2018, ApJ, 860, 90
Wang, L. J., Wang, X. F., Cano, Z., et al. 2019, MNRAS, 489, 1110
Whitesides, L., Lunnan, R., Kasliwal, M. M., et al. 2017, ApJ, 851, 107
Wilkinson, D. M., Maraston, C., Goddard, D., Thomas, D., & Parikh, T. 2017,
  MNRAS, 472, 4297
Xiang, D., Wang, X., Mo, J., et al. 2019, ApJ, 871, 176
Yokoo, T., Arimoto, J., Matsumoto, K., Takahashi, A., & Sadakane, K. 1994,
  PASJ, 46, L191
```